A century of observed temperature change in the Indian Ocean

Jacob O Wenegrat[1,1], Emma Bonanno[1,1], Ursula Rack[2,2], and Geoffrey Gebbie[3,3]

[1]University of Maryland, College Park
[2]University of Canterbury
[3]Woods Hole Oceanographic Institution

November 30, 2022

Abstract

The Indian Ocean is warming rapidly, with widespread effects on regional weather and global climate. Sea-surface temperature records indicate this warming trend extends back to the beginning of the 20th century, however the lack of a similarly long instrumental record of interior ocean temperatures leaves uncertainty around the subsurface trends. Here we utilize unique temperature observations from three historical German oceanographic expeditions of the late 19th and early 20th centuries: SMS Gazelle (1874–1876), Valdivia (1898–1899), and SMS Planet (1906–1907). These observations reveal a mean 20th century ocean warming that extends over the upper 750 m, and a spatial pattern of subsurface warming and cooling consistent with a 1°–2° southward shift of the southern subtropical gyre. These interior changes occurred largely over the last half of the 20th century, providing observational evidence for the acceleration of a multidecadal trend in subsurface Indian Ocean temperature.

A century of observed temperature change in the Indian Ocean

J.O. Wenegrat[1], E. Bonanno[1], U. Rack[2], and G. Gebbie [3]

[1]Department of Atmospheric and Oceanic Science, University of Maryland, College Park, USA
[2]School of Earth and Environment, University of Canterbury Christchurch, NZ
[3]Woods Hole Oceanographic Institution, Woods Hole, USA

Key Points:

- Historical observations of subsurface Indian Ocean temperature are recovered from expeditions in the late 19th and early 20th century
- Indian Ocean warming over the 20th century extends to 750 m depth
- Pattern of temperature change is consistent with surface warming and a poleward shift of the gyre over the last half of the 20th century

Corresponding author: Jacob O. Wenegrat, `wenegrat@umd.edu`

Abstract

The Indian Ocean is warming rapidly, with widespread effects on regional weather and global climate. Sea-surface temperature records indicate this warming trend extends back to the beginning of the 20th century, however the lack of a similarly long instrumental record of interior ocean temperatures leaves uncertainty around the subsurface trends. Here we utilize unique temperature observations from three historical German oceanographic expeditions of the late 19th and early 20th centuries: SMS *Gazelle* (1874–1876), *Valdivia* (1898–1899), and SMS *Planet* (1906–1907). These observations reveal a mean 20th century ocean warming that extends over the upper 750 m, and a spatial pattern of subsurface warming and cooling consistent with a 1°–2° southward shift of the southern subtropical gyre. These interior changes occurred largely over the last half of the 20th century, providing observational evidence for the acceleration of a multidecadal trend in subsurface Indian Ocean temperature.

Plain Language Summary

The Indian Ocean is warming rapidly, with far reaching effects on weather and climate. Sea-surface temperature records suggest this warming trend extends over the 20th century, however, similar long records of subsurface temperatures have not been available. Here we extend the observational record back more than a century using data from 3 historical oceanographic expeditions. These observations reveal a mean 20th century Indian Ocean warming that extends down to 750 m depth, as well as deep cooling in the subtropics. This provides evidence for the existence of a multidecadal trend in subsurface Indian Ocean temperatures that has accelerated over the last half of the 20th century.

1 Introduction

Sea-surface temperature (SST) in the Indian Ocean has warmed by approximately 1°C since 1950, among the fastest rate of increase in the global oceans (Roxy et al., 2014; Beal et al., 2019; Fox-Kemper et al., 2021). Ocean heat content also increased during this period at an accelerating rate, such that the Indian Ocean absorbed more than one-quarter of the total global ocean heat gain since 1990 (Levitus et al., 2012; Lee et al., 2015; Cheng et al., 2017), and close to half of the early 21st century heat increase in the upper 700 m (Desbruyères et al., 2017). This ocean heat uptake is believed to have modulated the rate of global surface air temperature increase (Lee et al., 2015; Nieves et al., 2015), underscoring the need for improved understanding of long-term heat storage in this region (Vialard, 2015). Ocean warming is also of particular consequence here—home to approximately one-third of the world's population—as many of the countries surrounding the Indian Ocean basin are vulnerable to sea-level rise and have high reliance on fisheries and rain-fed agriculture for food-security (Beal et al., 2020).

A challenge for understanding decadal to century timescale variability and change in the Indian Ocean is the lack of a long instrumental record of subsurface ocean temperatures. The modern observational record over the period spanning approximately 1960 to the present reveals that the rapid surface warming overlies a more heterogeneous pattern of warming and cooling below the thermocline (Alory et al., 2007). Disentangling long-term temperature trends using these modern observations is made more challenging by strong interannual and decadal variability, which is affected both by internal modes of variability such as the Indian Ocean Dipole, and remotely forced variability transmitted through both atmospheric teleconnections and heat transport through the Indonesian Throughflow (Han et al., 2014; Ummenhofer et al., 2017; Zhang et al., 2018; Ummenhofer et al., 2021). Thus, while reanalyses and proxy records indicate that SST warming occurred over the entire 20th century (Roxy et al., 2014; Tierney et al., 2015), it is currently unclear whether similar changes occurred in the subsurface ocean.

A unique opportunity for extending the instrumental record in time is revisiting the observations of early oceanographic expeditions of the 19th century, some of which took extensive subsurface temperature measurements. Comparison of the historical cruise data with modern observations can then be used to constrain changes in the interior ocean temperature over the last century. This approach has been used successfully for the Atlantic and Pacific oceans, where temperature records from the circumnavigation of the HMS *Challenger* (1872–1875) reveal warming that extends to below 1000 m depth (Roemmich et al., 2012), and mid-depth cooling in the Pacific attributable to the ongoing slow abyssal adjustment to the Little Ice Age (Gebbie & Huybers, 2019). The *Challenger* however did not sample extensively in the Indian Ocean during its circumnavigation, taking instead a southerly route crossing the Antarctic circle, leaving open the question of how the interior temperature in the Indian Ocean has changed over the 20th century.

Here we identify three German deep-sea expeditions of the late 19th and early 20th century that recorded temperature profiles in the Indian Ocean. These temperature measurements are digitized from the original cruise reports (Hydrographischen Amt des Reichs-Marine-Amts., 1889; Schott, 1902; Brennecke, 1909), and compared to modern temperature observations to provide a view into how the interior temperature structure of the Indian Ocean has changed over the last century. The earliest of the three cruises is the SMS *Gazelle*, a German corvette which undertook an eastabout scientific circumnavigation from 1874-1876, overlapping in time with the *Challenger* expedition, but with a route that transited the southern Indian Ocean (figure 1). This cruise was followed in 1898-1899 by the research vessel *Valdivia* which went deep into the Southern Ocean before returning north through the tropical Indian Ocean. The final cruise we consider is that of the SMS *Planet*, a survey ship which transited from Germany to Hong Kong in 1906–1907, with a route from the Cape of Good Hope to Madagascar and on to Indonesia. Together these cruises provide reasonable spatial coverage of the Indian Ocean south of 10°N—with more than 500 temperature observations at depths spanning from the surface to the bottom (figure 1e)—extending the available observational record back more than a century.

2 Data and Methods

2.1 Historical data

Historical observations from the *Gazelle*, *Valdivia*, and *Planet* were digitized from the original cruise reports (Hydrographischen Amt des Reichs-Marine-Amts., 1889; Schott, 1902; Brennecke, 1909). Data were double-entered independently and then checked for consistency. The historical data have a variety of unique quality control concerns relevant to calculating temperature changes, including issues related both to the accuracy of the temperature measurements themselves, and the positions at which they are reported. We document these below.

The *Gazelle* used mercury-column Miller-Casella thermometers for subsurface observations, as were used by the *Challenger* (Roemmich et al., 2012). These thermometers were of the 'min-max' type, using a sliding index to record the minimum and maximum water temperature encountered, and hence are inappropriate for use in regions with temperature inversions. Three stations with temperature inversions in the modern cli-

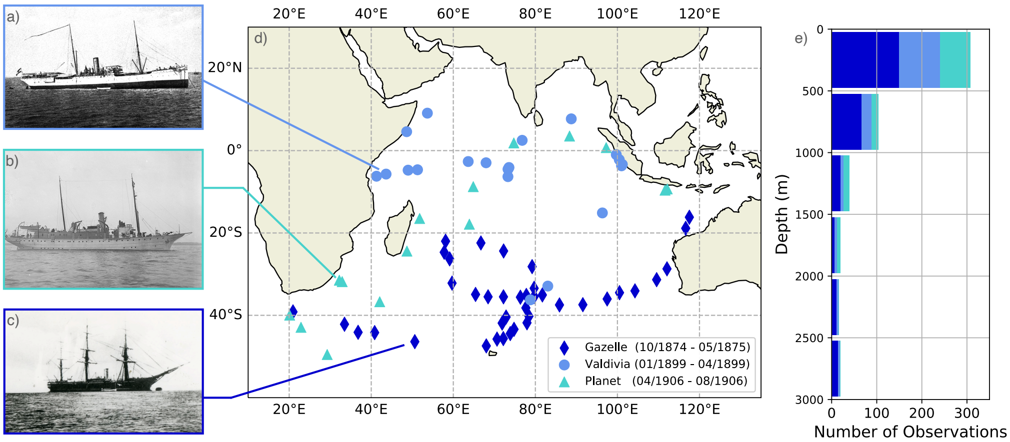

Figure 1. Overview of the Indian Ocean portion of the *Valdivia* (panel a, Chun, 1903), *Planet* (panel b, photo: *SLUB/Deutsche Fotothek, F. Stoedtner*), and *Gazelle* (panel c, photo: *Deutsches Schiffahrtsmuseum Fotoarchiv 94-2*) cruises. Stations used in this analysis are shown in panel d. A histogram of temperature observations as a function of depth is shown in panel e with color indicating the originating cruise following the color convention shown in the legend of panel d.

matology, and several historical measurements with apparent spurious reported temperature inversions, were removed from the analysis. The *Valdivia* and *Planet* also used min-max thermometers, however these were supplemented by Umkipp and Negretti-Zambra reversing thermometers (Wüst & Olson, 1933), and early Siemens deep-sea electric thermometers—which can all properly resolve non-monotonic temperature profiles. The reported temperature measurements do not clearly indicate which thermometer types were used for each observation, however visual inspection of the *Valdivia* and *Planet* observations, along with collocated modern data, did not indicate errors due to temperature inversions.

Mercury thermometers of both the min-max and reversing type are subject to errors from compression of the mercury at depth, which will tend to introduce a cold bias in the calculated difference between modern and historical records. G. Schott suggested a calibration formula for the *Valdivia* observations of $T(z) = T_m(z) - 0.011(T_m(0) - T_m(z))$, where $T(z)$ is the corrected temperature at a depth z, and T_m is the instrument measured temperature, such that the actual temperature at depth is adjusted to be colder depending on the difference between the measured temperature and the surface temperature (Wüst & Olson, 1933). This correction is however unlikely to be general, as the temperature-pressure relationship will vary across different temperature stratification profiles. An alternate, simpler, correction of 0.04°C km^{-1} was suggested by P. Tait for the *Challenger* instruments (Tait, 1882), which were similar in design to those used on the *Gazelle* and *Valdivia*. For the analysis here, which is generally limited to the upper 2 km, these corrections lead to only minor quantitative differences, and hence are not applied unless noted.

An additional source of uncertainty in the historical records—which cannot generally be quantified from the available cruise information—is the accuracy of the reported measurement positions, both in terms of the latitude and longitude of the station, and the depth of measurement. Positions estimated from celestial navigation and dead reckoning may include both systematic and random error of uncertain magnitude, but which are most likely to be important in regions of strong horizontal temperature gradients. Prior global analyses of high-temporal resolution (2-hour) historical surface data suggest the combined effect of uncertainty due to celestial navigation and dead-reckoning may introduce uncertainty in SST of order 0.1°C, increasing to 0.3°C in frontal regions (Dai et al., 2021). Systematic errors are estimated to be an order of magnitude smaller. It is unclear whether these estimates apply here as: (i) horizontal gradients of temperature are generally enhanced at the surface, suggesting SST-based estimates will overestimate the interior uncertainty, and (ii) estimated uncertainties depend on the time-elapsed between the observations and the last position fix by celestial navigation—information not clearly available for the stations used here. Given these uncertainties, and the coherent spatial patterns evident in the analysis of observations shown below, we do not attempt to explicitly account for errors in horizontal position.

Errors can also be introduced from the reported depths of the measurements, which were inferred based on the amount of line-out at the time of observation, rather than the modern approach of calculating measurement depth from the observed pressure at the instrument. This can lead to several, possibly competing, sources of bias. First, in the presence of strong currents the line can be deflected from the vertical, such that the actual measurement depth is shallower than reported (Wüst, 1933). This is most likely to be significant in regions of strong currents—we exclude one station from the *Valdivia* in the Agulhas where line deflections of 30° were noted—and will tend to introduce a warm bias in the historical observations, such that there will be a cold bias in the modern minus historical temperature differences. Secondly, although the *Valdivia* and *Planet* used wire for their measurements, the *Gazelle* used hemp line, which can stretch under the weight of the instruments and bottom weight. This might lead to shallow biases in the reported *Gazelle* measurement depths relative to the true depth of measurement, possibly introducing a warm bias in the modern minus *Gazelle* temperature differences. The errors in the basinwide mean temperature change due to line stretch are identically zero at the surface, and are estimated to increase approximately linearly to a maximum of 0.17°C at 750 m depth (supplementary information), below which they again decrease due to the weak interior temperature gradients. Errors of this magnitude are similar to the measurement uncertainty of the thermometers (Roemmich et al., 2012), and do not qualitatively affect our findings.

2.2 Comparison with modern data

We compare the historical observations to modern climatological values from the World Ocean Atlas (WOA) 2018 (Boyer et al., 2018). WOA incorporates extensive shipboard and profiling float measurements in a quality controlled and objectively analyzed climatology spanning the period of 2005–2017 at 0.25° horizontal resolution. The monthly 1° climatology for the period 1955–1964 is also used to isolate changes over the first half of the 20th century (section 3). In both cases, monthly temperature values are interpolated to the depth and horizontal position of the historical observations, and the difference between the modern and historical data is calculated. Below 1500 m depth monthly climatologies are unavailable and we instead use WOA seasonal climatologies. This approach limits the effect of seasonal variability on our calculated temperature differences, however clearly other timescales of variability may still be aliased into the *Gazelle*, *Valdivia*, and *Planet* observations, as discussed further below and in the supplementary information.

The mean historical-to-WOA temperature change is computed by a least squares method that accounts for measurement error and signals that are not representative of the decadal-mean temperature over the sampled region (figure 1). Full details of the method are provided in the supplementary information (and Gebbie & Huybers, 2019). Briefly, the contamination of the temperature observations is assumed to have three parts: (1) transient effects such as isopycnal heave due to internal waves or mesoscale eddies, (2) irregular spatial sampling of the basin, and (3) measurement or calibration error of the thermometers. The expected size of (1) varies spatially, with estimates taken from the WOCE Global Hydrographic Climatology (Gouretski & Koltermann, 2004), and corrected for the approximately 30 year time-interval of the historical observations. Following Gebbie and Huybers (2019) the variance due to (2) is assumed to be 20% that of transient motions (R. X. Huang, 2015), and the standard error due to (3) is assumed equal to 0.14°C (Roemmich et al., 2012). Results were tested and found to be qualitatively robust to parameter choices for the least-squares method, and similar to results using a simple arithmetic mean.

3 Results

Temperature differences between modern and historical data are calculated and a profile of the mean observed change over the last century in the Indian Ocean is shown in figure 2. SST has warmed by 0.87 (± 0.22) °C between the modern and historical observations (all uncertainties in this manuscript are reported as 2 standard deviations). This estimate is consistent with basin-averaged estimates from SST reanalyses. Near-surface warming decays away from the surface until a zero crossing near 750 m depth, somewhat shallower than what is observed from the *Challenger* observations in the Pacific where the warming signal reaches depths greater than a kilometer (Gebbie & Huybers, 2019). Weak cooling near 1500 m depth is also apparent in the mean profile, however the magnitude of the cooling is reduced if the Tait pressure correction is applied (dash-dot line in figure 2), suggesting this feature is at the detection limit of the observations.

These observations imply that ocean heat content over the upper 700 m increased by 4.8 (±2.2) $\times 10^{22}$ J over the 20th century (a rate of 0.40 [±0.18] $\times 10^{22}$ J/decade, see supplementary information). We show below that this increase in heat content occurred largely post-1955, implying a faster rate of change over the second half of the century. Direct comparison with prior estimates of heat content change in this region is confounded by differences in spatial coverage, as here we span the extent of the historical observations from 50° S to 9° N (figure 1). However for comparison, Levitus et al. (2012) estimated an increase of 0-700 m heat content of 3 $\times 10^{22}$ J for the Indian Ocean region (including the complete Indian sector of the Southern Ocean) over the period 1955-2010 (a linear trend of 0.5 $\times 10^{22}$ J/decade). This estimate is within the lower bound of our uncertainty range, and notably did not include the significant increase in heat con-

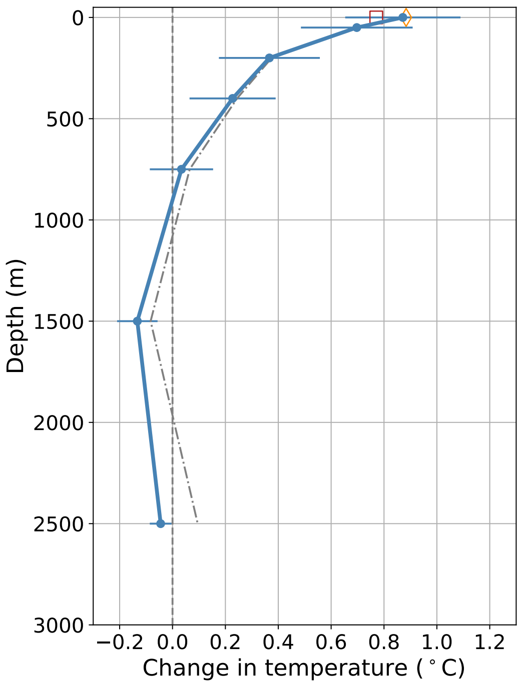

Figure 2. Profile of the observed mean temperature change in the Indian Ocean over the 20th century (blue line), with 95% confidence intervals. The mean profile with the Tait pressure correction (Tait, 1882) applied is shown by the thin dashed-dot line. Basin mean change in SST from the HadSST (orange diamond) and ERSST (red square) reanalyses are indicated at the surface.

tent between 2010-2017 which is included in our analysis (Cheng et al., 2017; Ummenhofer et al., 2020).

The basinwide average profile obscures significant horizontal spatial variability that is evident in depth-averaged maps (figure S1), and a meridional section formed by averaging observations in latitude and depth bins (figure 3, and supplementary information). The strongest warming in the latitude-depth slice is along the ACC subtropical front near 45°S, with an average near-surface value of approximately 1.5°C. Weaker warming of about 0.5°C also extends deeper than 600 m through much of the subtropical gyre, and above the thermocline in the tropics. A strip of near-surface cooling at 10°S extends down immediately below the thermocline, and along the poleward flank of the thermocline dome, with interior warming on the equatorward flank reaching deeper than 1000 m.

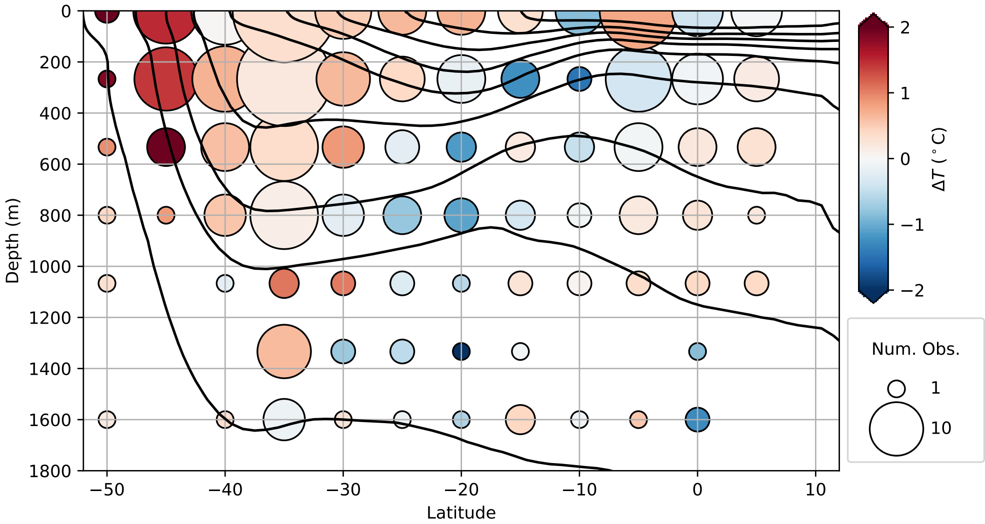

Figure 3. A latitude-depth slice indicates heterogeneous temperature change (colorscale) in the interior. Observations are binned into latitude-depth bins and averaged, with the number of observations in each bin indicated by the marker size (legend). Zonally averaged temperature contours from the 2005–2017 climatology are shown in black.

This pattern of temperature change over the last century is remarkably similar in structure to the temperature change noted in the modern observational record of the latter half of the 20th century (figure 4c, and Alory et al., 2007; L. Yang et al., 2020). It can largely be interpreted as resulting from a southward shift of the interior isotherms by approximately 1°–2° latitude, consistent with the latitudinal displacement of surface isotherms evident in SST reanalysis (figure 4a). This shift occurs in the second half of the century, and we note a recent analysis of *Gazelle* data found a similar temporal pattern for the increase of surface salinity in the Indian Ocean (Gould & Cunningham, 2021). Changes in surface values conflate both adiabatic and diabatic effects due to surface fluxes, however the implied shift of isotherms is sufficient in magnitude to explain many of the observed features in the interior temperature change, as is shown in figure 4d where an example zonally averaged temperature difference is created by shifting the modern temperature climatology by 1° latitude and differencing. Other features in the observed meridional structure of 20th century temperature change (figure 3) such as near-surface warming and cooling directly below the thermocline are not as well explained by shifting of the gyre position—but are again present in the recent observations (figure 4c)—and have been attributed to anthropogenic warming (Du & Xie, 2008; Dong et al., 2014; Swart et al., 2018), changes in heat advection from the Pacific through the Indonesian Throughflow (Alory et al., 2007; Ummenhofer et al., 2017), and Southern Ocean ventilation (L. Yang et al., 2020).

The similarity of the structure of the total 20th century temperature change to that observed over only the period 1955–2017 suggests that interior temperature changes before mid-century may have been limited. We show the mean temperature change at 250 m depth from the ECMWF Ensemble of Ocean Reanalyses of the 20th century (ORA-20C, de Boisséson et al., 2018)—a 10-member ensemble of data assimilating global simulations that span the period 1900-2009—in figure 4b. Reanalyses can be biased by changing data availability over time (de Boisseson & Balmaseda, 2016), however comparisons to the observations are informative. In the reanalysis the first-half of the century is characterized by weak interior warming, relative to the 1900-1910 mean. However, beginning around 1970 there is a transition to a meridional dipole pattern of warming and cooling, indicating that the mid-century acceleration of surface warming (Roxy et al., 2014), and the southward shift of surface isotherms, extended into the subsurface ocean.

To confirm this interpretation, we calculate the temperature difference over just the first half of the 20th century by subtracting the historical measurements from the WOA 1955–1964 observational climatology. This shows limited evidence of interior temperature change over this period (figures 5 and S2), with a statistically insignificant change in estimated ocean heat content over the upper 700 m (-0.7 $[\pm 2.2]$ $\times 10^{22}$ J, a rate of -0.10 $[\pm 0.30]$ $\times 10^{22}$ J/decade). This suggests that surface warming beginning around 1900 or earlier—evident in SST reanalyses and paleoreconstructions (figure 5 and Abram et al., 2016; Tierney et al., 2015)—may not have extended into the interior until after mid-century. Mean subsurface cooling below 500 m depth originates in these observations from apparent cooling along the ACC and the poleward flank of the thermocline dome (figure S2), and may contribute to the observed cooling near 1500 m in figure 2. Most of the observed changes in subsurface temperature above the thermocline between 1874 and 2017 (eg. figure 2) thus appear to have occurred in the last half of the 20th century.

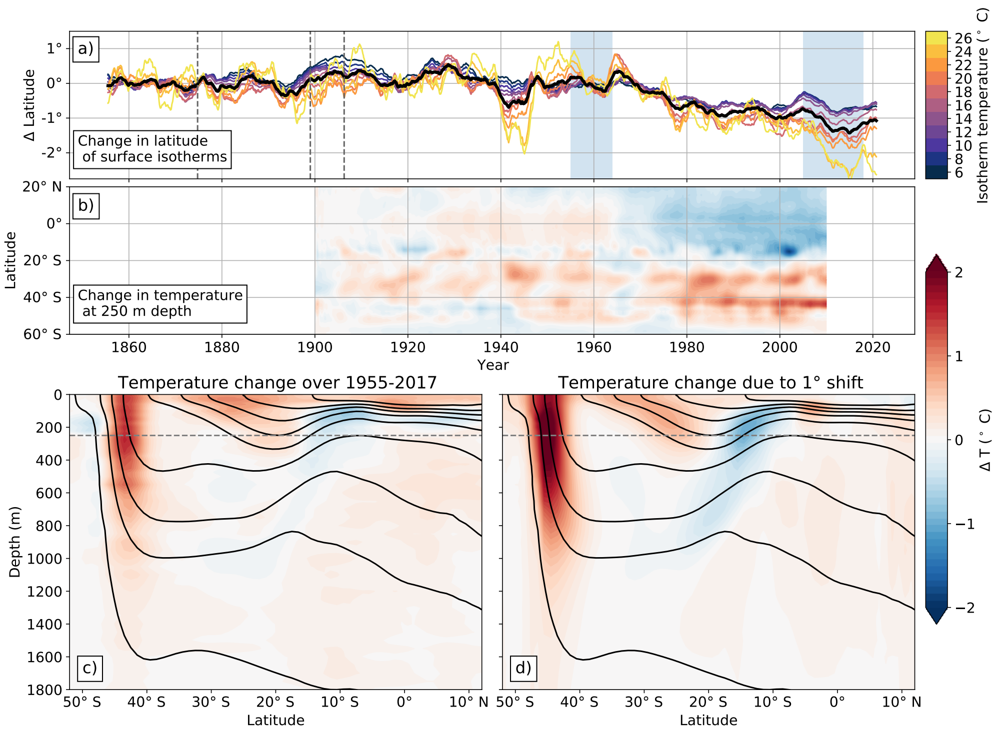

Figure 4. Indian Ocean temperature change has accelerated over the last half of the 20th century. a) Time series of the change in mean latitude of surface isotherms (colored lines) in the ERSST reanalysis (zonally averaged and smoothed with a 3 year running mean), referenced relative to the 1860-1870 average position. Mean surface isotherm displacement is shown by the heavy black line, the thin dashed gray lines indicate the time of the 3 historical cruises, and the climatological periods of 1955-1964 and 2005-2017 are indicated by light blue shading. b) Ensemble mean temperature at 250 m depth from the ORA-20C reanalysis (de Boisséson et al., 2018), referenced relative to the 1900-1910 mean at each latitude. c) Climatological change in temperature between 1955 and 2017 from observations (WOA). d) Temperature change inferred by shifting the modern climatological values by 1°S, consistent with the surface isotherm displacement. In panels b-d the temperature is zonally averaged over 60°E - 100°E, and in c and d the black contours indicate the modern average temperature field while the dashed gray line indicates 250 m depth for comparison with panel b.

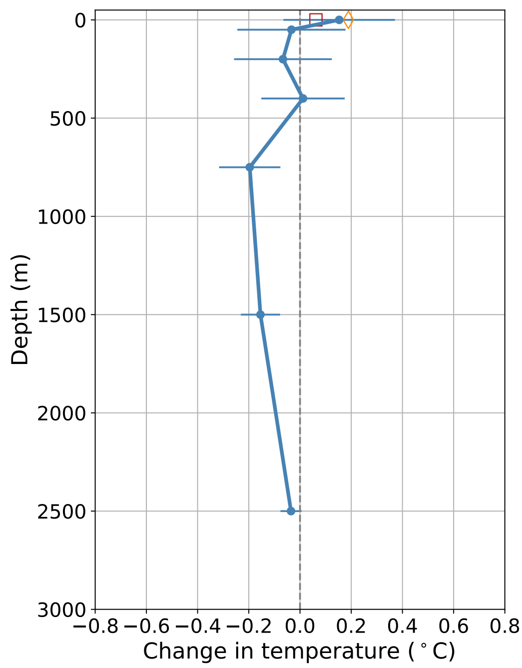

Figure 5. As in figure 2, but for the observed temperature change between the historical cruises and the 1955-1964 climatological values.

4 Summary

The Indian Ocean is recognized to play a major role in both regional and global climate, with SST and ocean heat content increasing at a rate exceeding many other parts of the global oceans. Despite this, quantifying long-term subsurface temperature trends has been made difficult by the relatively short period ($\sim$60 years) of available interior ocean temperature measurements. Here we have utilized a unique dataset of late 19th and early 20th century oceanographic expeditions to extend the observational record back to the period spanning 1874–1906. Results of this suggest a pattern of mean 20th century warming in the Indian Ocean that extends to 750 m depth, similar to what was observed from the *Challenger* expedition in the Pacific (Roemmich et al., 2012; Gebbie & Huybers, 2019).

The interior temperature changes in the Indian Ocean appear to have occurred predominantly in the last half of the 20th century, with only limited change in temperature between the historical measurements and the 1955–1964 climatological values. This is true both for the mean warming profile (cf. figures 2 and 5), and the latitude-depth pattern of 20th century temperature change (figure 3), which is closely similar to the pattern of change seen in just the modern observational record post-1960 (Alory et al., 2007). These observations thus suggest that increases in SST over the first half of the 20th century—also evident in this data—were not necessarily associated with significant interior warming. This finding is consistent with recent results showing that, despite the long-term warming trend in SST, ocean heat content in the Indian Ocean was relatively stable until the 1990s, after which the Indian Ocean began to play a major role in global ocean heat uptake (Lee et al., 2015; Cheng et al., 2017; Desbruyères et al., 2017).

Long-term warming trends in the Indian Ocean have been shown in modeling studies to be the result of anthropogenic forcing (Du & Xie, 2008; Dong et al., 2014). The ocean response is however mediated through a variety of mechanisms that include changes in heat advection through the Indonesian throughflow (Alory et al., 2007; Schwarzkopf & Böning, 2011; Ummenhofer et al., 2017), ventilation from the southern ocean (Jayasankar et al., 2019; L. Yang et al., 2020), and the coupled atmosphere-ocean circulation (Xie et al., 2010; H. Yang et al., 2020). Significant uncertainty thus persists in the understanding of regional and subsurface trends, further confounded by the relative scarcity of available long-term subsurface temperature measurements (Gopika et al., 2020; Beal et al., 2020; Ummenhofer et al., 2021). Here we have utilized unique historical observations to extend the available observations back more than a century, providing an independent line of evidence for multidecadal temperature change in the Indian Ocean, that extends into the subsurface interior, and that has largely occurred over the last half of the 20th century.

Acknowledgments

The authors acknowledge the effort of many that went into collecting the invaluable data of the *Gazelle*, *Valdivia*, and *Planet*—including many who perished on these voyages. The accessibility of this data, well over a century since it was collected, sets a benchmark for our collective modern efforts. However, we believe it important to acknowledge that these historical expeditions also involved other goals, scientific and political, that were likely harmful to many they encountered, and hence any consideration of their legacy must include a holistic consideration of their impact and historical context. The authors thank Julia Wenegrat for help with digitizing the historical records, the Biodiversity Heritage Library (https://www.biodiversitylibrary.org/) for making available online scanned versions of the original cruise reports, and the Deutsches Schiffahrtsmuseum for assistance locating photographs of the *Gazelle*. GG is supported by U.S. NSF-OCE 82280500. Insightful suggestions from Mike McPhaden and Raghu Murtugudde during preparation of this manuscript are gratefully acknowledged.

Open Research

Archiving of digitized data from the *Gazelle*, *Valdivia*, and *Planet* used in this analysis is in progress, and will be made publicly available in csv and netcdf format through `zenodo.org` upon manuscript acceptance. Data is made available now as supplementary information for purposes of the review process. All analysis code used in the manuscript will also be made publicly available through `zenodo.org`. World Ocean Atlas data is available at: `https://www.ncei.noaa.gov/products/world-ocean-atlas`. ERSST v5 reanalysis output (B. Huang et al., 2017) from: `https://www.ncei.noaa.gov/products/extended-reconstructed-sst`. HadSST v4.0.1 reanalysis output (Kennedy et al., 2019) from: `https://www.metoffice.gov.uk/hadobs/hadsst4/`. ORA-20C reanalysis (de Boisséson et al., 2018) from: `https://www.cen.uni-hamburg.de/en/icdc/data/ocean/easy-init-ocean/ecmwf-ensemble-of-ocean-reanalyses-of-the-20th-century-ora-20c.html`.

References

Abram, N. J., McGregor, H. V., Tierney, J. E., Evans, M. N., McKay, N. P., Kaufman, D. S., & the PAGES 2k Consortium. (2016, August). Early onset of industrial-era warming across the oceans and continents. *Nature*, *536*(7617), 411–418. Retrieved 2022-02-03, from `http://www.nature.com/articles/nature19082` doi: 10.1038/nature19082

Alory, G., Wijffels, S., & Meyers, G. (2007, January). Observed temperature trends in the Indian Ocean over 1960–1999 and associated mechanisms. *Geophysical Research Letters*, *34*(2), L02606. Retrieved 2021-07-12, from `https://onlinelibrary.wiley.com/doi/10.1029/2006GL028044` doi: 10.1029/2006GL028044

Beal, L. M., Vialard, J., & Roxy, M. K. (2019, December). *Full Report. IndOOS-2: A roadmap to sustained observations of the Indian Ocean for 2020-2030* (Tech. Rep.). CLIVAR. Retrieved 2022-04-22, from `http://www.clivar.org/sites/default/files/documents/IndOOS_report_small.pdf` doi: 10.36071/clivar.rp.4.2019

Beal, L. M., Vialard, J., Roxy, M. K., Li, J., Andres, M., Annamalai, H., ... Parvathi, V. (2020, November). A Road Map to IndOOS-2: Better Observations of the Rapidly Warming Indian Ocean. *Bulletin of the American Meteorological Society*, *101*(11), E1891–E1913. Retrieved 2022-04-21, from https://journals.ametsoc.org/view/journals/bams/101/11/bamsD190209.xml doi: 10.1175/BAMS-D-19-0209.1

Boyer, T., Baranova, O., Coleman, C., Garcia, H., Grodsky, A., Locarnini, R., ... Zweng, M. (2018). *World Ocean Database 2018* (Tech. Rep.).

Brennecke, W. (1909). *Forschungrsreise S.M.S. "Planet" 1906/1907, III. Band Ozeanographie.* Berlin: Verlag von Karl Siegismund.

Cheng, L., Trenberth, K. E., Fasullo, J., Boyer, T., Abraham, J., & Zhu, J. (2017, March). Improved estimates of ocean heat content from 1960 to 2015. *Science Advances*, *3*(3), e1601545. Retrieved 2022-04-20, from https://www.science.org/doi/10.1126/sciadv.1601545 doi: 10.1126/sciadv.1601545

Chun, K. (1903). *Aus den tiefen des weltmeeres, von Carl Chun. Schilderungen von der Deutschen tiefsee-expedition.* Jena,: G. Fischer,. Retrieved 2021-07-19, from http://www.biodiversitylibrary.org/bibliography/14876 doi: 10.5962/bhl.title.14876

Dai, C., Chan, D., Huybers, P., & Pillai, N. (2021, March). Late 19th century navigational uncertainties and their influence on sea surface temperature estimates. *The Annals of Applied Statistics*, *15*(1). Retrieved 2021-07-12, from https://projecteuclid.org/journals/annals-of-applied-statistics/volume-15/issue-1/Late-19th-century-navigational-uncertainties-and-their-influence-on-sea/10.1214/20-AOAS1367.full doi: 10.1214/20-AOAS1367

de Boisseson, E., & Balmaseda, M. A. (2016). *An ensemble of 20th century ocean reanalyses for providing ocean initial conditions for CERA-20C coupled streams.* (Tech. Rep. No. 24). ECMWF.

de Boisséson, E., Balmaseda, M. A., & Mayer, M. (2018, May). Ocean heat content variability in an ensemble of twentieth century ocean reanalyses. *Climate Dynamics*, *50*(9-10), 3783–3798. Retrieved 2021-07-22, from http://link.springer.com/10.1007/s00382-017-3845-0 doi: 10.1007/s00382-017-3845-0

Desbruyères, D., McDonagh, E. L., King, B. A., & Thierry, V. (2017, March). Global and Full-Depth Ocean Temperature Trends during the Early Twenty-First Century from Argo and Repeat Hydrography. *Journal of Climate*, *30*(6), 1985–1997. Retrieved 2022-04-20, from https://journals.ametsoc.org/doi/10.1175/JCLI-D-16-0396.1 doi: 10.1175/JCLI-D-16-0396.1

Dong, L., Zhou, T., & Wu, B. (2014, January). Indian Ocean warming during 1958–2004 simulated by a climate system model and its mechanism. *Climate Dynamics*, *42*(1-2), 203–217. Retrieved 2021-07-12, from http://link.springer.com/10.1007/s00382-013-1722-z doi: 10.1007/s00382-013-1722-z

Du, Y., & Xie, S.-P. (2008, April). Role of atmospheric adjustments in the tropical Indian Ocean warming during the 20th century in climate models. *Geophysical Research Letters*, *35*(8), L08712. Retrieved 2022-04-22, from http://doi.wiley.com/10.1029/2008GL033631 doi: 10.1029/2008GL033631

Fox-Kemper, B., Hewitt, H. T., Xiao, C., Aalgeirsdóttir, G., Drijfhout, S. S., Edwards, T. L., ... Yu, Y. (2021). Ocean, cryosphere, and sea level change. In V. Masson-Delmotte et al. (Eds.), *Climate Change 2021: The Physical Science Basis. Contribution of Working Group I to the Sixth Assessment Report of the Intergovernmental Panel on Climate Change.* Cambridge University Press.

Gebbie, G., & Huybers, P. (2010, August). Total Matrix Intercomparison: A Method for Determining the Geometry of Water-Mass Pathways. *Journal of Physical Oceanography*, *40*(8), 1710–1728. Retrieved 2022-02-02, from http://journals.ametsoc.org/doi/10.1175/2010JPO4272.1 doi: 10.1175/2010JPO4272.1

Gebbie, G., & Huybers, P. (2019, January). The Little Ice Age and 20th-century deep Pacific cooling. *Science*, *363*(6422), 70–74. Retrieved 2021-07-12, from https://www.sciencemag.org/lookup/doi/10.1126/science.aar8413 doi: 10.1126/science.aar8413

Gergis, J. L., & Fowler, A. M. (2009, February). A history of ENSO events since A.D. 1525: implications for future climate change. *Climatic Change*, *92*(3-4), 343–387. Retrieved 2021-07-17, from http://link.springer.com/10.1007/s10584-008-9476-z doi: 10.1007/s10584-008-9476-z

Gopika, S., Izumo, T., Vialard, J., Lengaigne, M., Suresh, I., & Kumar, M. R. R.

(2020, January). Aliasing of the Indian Ocean externally-forced warming spatial pattern by internal climate variability. *Climate Dynamics*, *54*(1-2), 1093–1111. Retrieved 2022-04-22, from http://link.springer.com/10.1007/s00382-019-05049-9 doi: 10.1007/s00382-019-05049-9

Gould, W. J., & Cunningham, S. A. (2021, December). Global-scale patterns of observed sea surface salinity intensified since the 1870s. *Communications Earth & Environment*, *2*(1), 76. Retrieved 2022-02-03, from http://www.nature.com/articles/s43247-021-00161-3 doi: 10.1038/s43247-021-00161-3

Gouretski, V., & Koltermann, K. (2004). *WOCE Global Hydrographic Climatology* (Tech. Rep. No. 35). Berichte des Bundesamtes für Seeschifffahrt und Hydrographie.

Han, W., Vialard, J., McPhaden, M. J., Lee, T., Masumoto, Y., Feng, M., & de Ruijter, W. P. (2014, November). Indian Ocean Decadal Variability: A Review. *Bulletin of the American Meteorological Society*, *95*(11), 1679–1703. Retrieved 2021-07-12, from https://journals.ametsoc.org/doi/10.1175/BAMS-D-13-00028.1 doi: 10.1175/BAMS-D-13-00028.1

Huang, B., Thorne, P. W., Banzon, V. F., Boyer, T., Chepurin, G., Lawrimore, J. H., ... Zhang, H.-M. (2017). *NOAA Extended Reconstructed Sea Surface Temperature (ERSST), Version 5.* NOAA National Centers for Environmental Information. Retrieved 2022-01-25, from https://data.nodc.noaa.gov/cgi-bin/iso?id=gov.noaa.ncdc:C00927 (Type: dataset) doi: 10.7289/V5T72FNM

Huang, R. X. (2015, December). Heaving modes in the world oceans. *Climate Dynamics*, *45*(11-12), 3563–3591. Retrieved 2022-01-25, from http://link.springer.com/10.1007/s00382-015-2557-6 doi: 10.1007/s00382-015-2557-6

Hydrographischen Amt des Reichs-Marine-Amts. (1889). *Die Forschungsreise S. M. S. "Gazelle" in den Jahren 1874 bis 1876 : unter Kommando des Kapitän See Freiherrn von Schleinitz / herausgegeben von dem Hydrogrphischen Amt des Reishs-Marine-Amts.* Berlin :: E. S. Mittler und Sohn,. Retrieved 2022-01-26, from http://www.biodiversitylibrary.org/bibliography/984 doi: 10.5962/bhl.title.984

Jayasankar, T., Murtugudde, R., & Eldho, T. (2019, November). The Indian Ocean

Deep Meridional Overturning Circulation in Three Ocean Reanalysis Products. *Geophysical Research Letters*, *46*(21), 12146–12155. Retrieved 2021-07-12, from https://onlinelibrary.wiley.com/doi/10.1029/2019GL084244 doi: 10.1029/2019GL084244

Kennedy, J. J., Rayner, N. A., Atkinson, C. P., & Killick, R. E. (2019, July). An Ensemble Data Set of Sea Surface Temperature Change From 1850: The Met Office Hadley Centre HadSST.4.0.0.0 Data Set. *Journal of Geophysical Research: Atmospheres*, *124*(14), 7719–7763. Retrieved 2022-01-25, from https://onlinelibrary.wiley.com/doi/abs/10.1029/2018JD029867 doi: 10.1029/2018JD029867

Lee, S.-K., Park, W., Baringer, M. O., Gordon, A. L., Huber, B., & Liu, Y. (2015, June). Pacific origin of the abrupt increase in Indian Ocean heat content during the warming hiatus. *Nature Geoscience*, *8*(6), 445–449. Retrieved 2021-07-16, from http://www.nature.com/articles/ngeo2438 doi: 10.1038/ngeo2438

Levitus, S., Antonov, J. I., Boyer, T. P., Baranova, O. K., Garcia, H. E., Locarnini, R. A., ... Zweng, M. M. (2012, May). World ocean heat content and thermosteric sea level change (0-2000 m), 1955-2010. *Geophysical Research Letters*, *39*(10), n/a–n/a. Retrieved 2022-04-20, from http://doi.wiley.com/10.1029/2012GL051106 doi: 10.1029/2012GL051106

Nieves, V., Willis, J. K., & Patzert, W. C. (2015, July). Recent hiatus caused by decadal shift in Indo-Pacific heating. *Science*, *349*(6247), 532–535. Retrieved 2022-04-22, from https://www.science.org/doi/10.1126/science.aaa4521 doi: 10.1126/science.aaa4521

Roemmich, D., John Gould, W., & Gilson, J. (2012, June). 135 years of global ocean warming between the Challenger expedition and the Argo Programme. *Nature Climate Change*, *2*(6), 425–428. Retrieved 2021-07-12, from http://www.nature.com/articles/nclimate1461 doi: 10.1038/nclimate1461

Roxy, M. K., Ritika, K., Terray, P., & Masson, S. (2014, November). The Curious Case of Indian Ocean Warming. *Journal of Climate*, *27*(22), 8501–8509. Retrieved 2021-07-12, from http://journals.ametsoc.org/doi/10.1175/JCLI-D-14-00471.1 doi: 10.1175/JCLI-D-14-00471.1

Saji, N., & Yamagata, T. (2003). Possible impacts of Indian Ocean Dipole mode events on global climate. *Climate Research*, *25*, 151–169. Retrieved 2021-07-16, from http://www.int-res.com/abstracts/cr/v25/n2/p151-169/ doi: 10.3354/cr025151

Saji, N. H., Goswami, B. N., Vinayachandran, P. N., & Yamagata, T. (1999, September). A dipole mode in the tropical Indian Ocean. *Nature*, *401*(6751), 360–363. Retrieved 2021-07-16, from http://www.nature.com/articles/43854 doi: 10.1038/43854

Schott, G. (1902). *Oceanographie und maritime Meteorologie* (Vol. 1). Jena, G. Fischer.

Schwarzkopf, F. U., & Böning, C. W. (2011, June). Contribution of Pacific wind stress to multi-decadal variations in upper-ocean heat content and sea level in the tropical south Indian Ocean. *Geophysical Research Letters*, *38*(12). Retrieved 2021-07-12, from https://onlinelibrary.wiley.com/doi/10.1029/2011GL047651 doi: 10.1029/2011GL047651

Swart, N. C., Gille, S. T., Fyfe, J. C., & Gillett, N. P. (2018, November). Recent Southern Ocean warming and freshening driven by greenhouse gas emissions and ozone depletion. *Nature Geoscience*, *11*(11), 836–841. Retrieved 2022-04-22, from http://www.nature.com/articles/s41561-018-0226-1 doi: 10.1038/s41561-018-0226-1

Tait, P. (1882). *The Pressure Errors of the Challenger Thermometers* (Tech. Rep. Nos. Vol. II, Appendix A). HM Stationary Office.

Tierney, J. E., Abram, N. J., Anchukaitis, K. J., Evans, M. N., Giry, C., Kilbourne, K. H., … Zinke, J. (2015, March). Tropical sea surface temperatures for the past four centuries reconstructed from coral archives. *Paleoceanography*, *30*(3), 226–252. Retrieved 2022-02-03, from http://doi.wiley.com/10.1002/2014PA002717 doi: 10.1002/2014PA002717

Ummenhofer, C. C., Biastoch, A., & Böning, C. W. (2017, March). Multidecadal Indian Ocean Variability Linked to the Pacific and Implications for Preconditioning Indian Ocean Dipole Events. *Journal of Climate*, *30*(5), 1739–1751. Retrieved 2021-07-12, from http://journals.ametsoc.org/doi/10.1175/JCLI-D-16-0200.1 doi: 10.1175/JCLI-D-16-0200.1

Ummenhofer, C. C., Murty, S. A., Sprintall, J., Lee, T., & Abram, N. J. (2021, August). Heat and freshwater changes in the Indian Ocean region. *Na-*

ture Reviews Earth & Environment, *2*(8), 525–541. Retrieved 2022-02-03, from https://www.nature.com/articles/s43017-021-00192-6 doi: 10.1038/s43017-021-00192-6

Ummenhofer, C. C., Ryan, S., England, M. H., Scheinert, M., Wagner, P., Biastoch, A., & Böning, C. W. (2020, November). Late 20th Century Indian Ocean Heat Content Gain Masked by Wind Forcing. *Geophysical Research Letters*, *47*(22). Retrieved 2022-04-22, from https://onlinelibrary.wiley.com/doi/10.1029/2020GL088692 doi: 10.1029/2020GL088692

Vialard, J. (2015, June). Hiatus heat in the Indian Ocean. *Nature Geoscience*, *8*(6), 423–424. Retrieved 2022-04-22, from http://www.nature.com/articles/ngeo2442 doi: 10.1038/ngeo2442

Wilks, D. S. (2016, December). "The Stippling Shows Statistically Significant Grid Points": How Research Results are Routinely Overstated and Overinterpreted, and What to Do about It. *Bulletin of the American Meteorological Society*, *97*(12), 2263–2273. Retrieved 2021-07-22, from https://journals.ametsoc.org/doi/10.1175/BAMS-D-15-00267.1 doi: 10.1175/BAMS-D-15-00267.1

Wortham, C., & Wunsch, C. (2014, March). A Multidimensional Spectral Description of Ocean Variability. *Journal of Physical Oceanography*, *44*(3), 944–966. Retrieved 2022-02-02, from http://journals.ametsoc.org/doi/10.1175/JPO-D-13-0113.1 doi: 10.1175/JPO-D-13-0113.1

Wüst, G. (1933). Thermometric Measurement of Depth. *International Hydrographic Review*, *10*(1), 28–49.

Wüst, G., & Olson, B. (1933). *Das Bodenwasser und die Gliederung der atlantischen Tiefsee.* (Tech. Rep. No. 6). Berlin.

Xie, S.-P., Deser, C., Vecchi, G. A., Ma, J., Teng, H., & Wittenberg, A. T. (2010, February). Global Warming Pattern Formation: Sea Surface Temperature and Rainfall*. *Journal of Climate*, *23*(4), 966–986. Retrieved 2022-04-22, from http://journals.ametsoc.org/doi/10.1175/2009JCLI3329.1 doi: 10.1175/2009JCLI3329.1

Yang, H., Lohmann, G., Krebs-Kanzow, U., Ionita, M., Shi, X., Sidorenko, D., … Gowan, E. J. (2020, March). Poleward Shift of the Major Ocean Gyres Detected in a Warming Climate. *Geophysical Research Letters*, *47*(5). Retrieved 2021-07-12, from https://onlinelibrary.wiley.com/doi/10.1029/2019GL085868 doi: 10.1029/2019GL085868

Yang, L., Murtugudde, R., Zhou, L., & Liang, P. (2020, December). A Potential Link Between the Southern Ocean Warming and the South Indian Ocean Heat Balance. *Journal of Geophysical Research: Oceans*, *125*(12). Retrieved 2021-07-12, from https://onlinelibrary.wiley.com/doi/10.1029/2020JC016132 doi: 10.1029/2020JC016132

Zhang, Y., Feng, M., Du, Y., Phillips, H. E., Bindoff, N. L., & McPhaden, M. J. (2018). Strengthened Indonesian Throughflow Drives Decadal Warming in the Southern Indian Ocean. *Geophysical Research Letters*, *45*(12), 6167–6175. Retrieved 2021-07-12, from https://onlinelibrary.wiley.com/doi/10.1029/2018GL078265 doi: 10.1029/2018GL078265

Supporting Information for "A century of observed temperature change in the Indian Ocean"

J.O. Wenegrat[1], E. Bonanno[1], U. Rack[2], and G. Gebbie [3]

[1]Department of Atmospheric and Oceanic Science, University of Maryland, College Park, USA

[2]School of Earth and Environment, University of Canterbury Christchurch, NZ

[3]Woods Hole Oceanographic Institution, Woods Hole, USA

Contents of this file

1. Text S1 to S4
2. Figures S1 to S8

Introduction

This document contains supporting information for Wenegrat et al. 'A century of observed temperature change in the Indian Ocean', under review for publication in *Geophysical Research Letters*.

Text S1: Vertical profile of temperature difference

Basinwide average profiles are calculated following the method detailed in Gebbie and Huybers (2019, their supplementary information S5.4), as updated here.

The temperature difference between the historical observations and the corresponding World Ocean Atlas (WOA) value is,

$$\Delta T(r_i) = T(r_i, t_w) - T(r_i, t_h), \tag{1}$$

where $T(r_i, t_h)$ is the ith *historical* temperature observation at location, r_i, and time, t_h, and $T(r_i, t_w)$ is the WOA temperature at the same location. The observations are combined into a vector,

$$\mathbf{\Delta T} = \begin{pmatrix} \Delta T(r_1) \\ \Delta T(r_2) \\ \vdots \\ \Delta T(r_M) \end{pmatrix}. \tag{2}$$

Temperature changes at a given pressure are assumed equivalent to potential temperature changes.

Basinwide-average temperature profiles:

Our goal is to extract the decadal signal of water-mass change from the historical temperature observations

$$\overline{\mathbf{\Delta T}} = \begin{pmatrix} \overline{\Delta\theta(z_1)} \\ \overline{\Delta\theta(z_2)} \\ \vdots \\ \overline{\Delta\theta(z_K)} \end{pmatrix}, \tag{3}$$

where we have defined a grid of K depths. Given knowledge of the basinwide averages, one can make a prediction for each WOA−historical temperature difference,

$$\mathbf{\Delta T} = \mathbf{H}\overline{\mathbf{\Delta T}} + \mathbf{q}, \tag{4}$$

where $\mathbf{H}$ maps the basinwide mean onto the observational point by noting the basin of the observations and vertical linear interpolation, $\mathbf{q}$ is contamination by measurement error and signals that are not representative of the decadal-mean, basinwide-average temperature. The contamination is decomposed into three parts,

$$\mathbf{q} = \mathbf{n}_T + \mathbf{n}_S + \mathbf{n}_M, \tag{5}$$

where $\mathbf{n}_T$ is contamination by transient effects such as isopycnal heave due to internal waves or mesoscale eddies, $\mathbf{n}_S$ is due to the irregular spatial sampling of each basin, and $\mathbf{n}_M$ is measurement or calibration error of the thermometer. Note that no depth correction is made here, and temperature differences may be biased toward warming (as discussed below in section S2).

The expected size of $\mathbf{n}_T$ is related to the energy in the interannual and higher-frequency bands. We use estimates from the WOCE Global Hydrographic Climatology (Gouretski & Koltermann, 2004) to quantify this error and its spatial pattern. Errors that primarily reflect an uncertainty due to a representativity error were previously estimated in this climatology, where the magnitude of interannual temperature variability is 1.6°C at the surface, decreasing to 0.8°C below the mixed layer, and 0.02°C at 3000 meters depth. Inherent in their mapping is a horizontal lengthscale of $L_{xy}^T = 450$ km. This corresponds to a vertical lengthscale of $L_z^T = 450$ meters when applying an aspect ratio based upon mean depth and lateral extent of the ocean. Their mapping is the degree of error necessary to place the non-synoptic cruises of a 10-year time interval into a coherent picture. Estimated errors are similar to those of (Wortham & Wunsch, 2014), who also note that the spatial scales increase as the temporal scales increase. Above 1300 meters depth, the aliased variability is typically larger than the measurement error described below.

Next we describe the second moment matrix of temporal contamination, $\mathbf{R}_{TT} =< \mathbf{n}_T(\mathbf{n}_T)^T >$. Note that $\mathbf{n}_T$ depends on the difference of contamination during the two time periods, $n_T(r_i) = \eta_T(r_i, t_w) - \eta_T(r_i, t_h)$, where $\eta_T(r, t)$ is the difference between temperature at a given time and the decadal average. The WGHC statistics give the error covariance for $\eta_T(r, t_w)$ not $n_T(r)$. This covariance matrix is reconstructed by first creating a correlation matrix,

$$\mathbf{R}_\rho = \begin{pmatrix} \rho(0) & \rho(\delta) & \rho(2\delta) & \dots & \\ \rho(\delta) & \rho(0) & \rho(\delta) & \dots & \\ \rho(2\delta) & \rho(\delta) & \rho(0) & \dots & \\ \vdots & \vdots & \vdots & \ddots & \\ & & & & \rho(0) \end{pmatrix}, \tag{6}$$

where the autocorrelation function, $\rho(\delta)$, is given by a Gaussian with a horizontal lengthscale of 450 km and a vertical lengthscale of 450 meters. We derive the covariance matrix by pre- and post-multiplying the correlation matrix, $\mathbf{R}_{\eta\eta} = \boldsymbol{\sigma}_\eta \boldsymbol{\sigma}_\eta^T \circ \mathbf{R}_\rho$, where $\boldsymbol{\sigma}_\eta$ is the vector of the standard deviation of the WGHC interannual variability and $\circ$ is the Hadamard product. Here the time interval of the historical cruises is about 30 years, or three times as long as the WOCE era. Due to the red spectrum of ocean variability, the potential for aliased variability over this longer time interval is increased. To get a better constraint on T_{ratio}, we have to assume a frequency spectrum. If we assume the power density spectrum is red with a power law of f^{-2}, then we can integrate to determine the variance at frequencies greater than 1/(30 yr) and 1/(10 yr). The variance at frequencies greater than f is proportional to 1/f, so the ratio of variance greater than 1/(30 yr) to that greater than 1/(10 yr) is $T_{ratio} = 30/10 = 3$. Both the modern and historical intervals have variability and are assumed to be statistically independent, and thus, $\mathbf{R}_{TT} = (T_{ratio} + 1)\mathbf{R}_{\eta\eta}$.

We assume that the variance due to spatial water-mass variability, i.e., $\mathbf{R}_{SS} =< \mathbf{n}_S(\mathbf{n}_S)^T >$, has a magnitude that is 20% that of the temporal variability as the local water-mass variability on interannual scales is dwarfed by heaving motions (Huang, 2015). The relevant parameter is $S_{ratio} = 0.2$. These water-mass variations are assumed to have a larger spatial scale ($L_{xy}^S = 2000$ km horizontally, $L_z^S = 1$ km vertically), as seen in an evaluation of water-mass fractions on an isobaric surface (Gebbie & Huybers, 2010). Accounting for this spatial variability has the potential to increase the final error of our estimates by taking into account biases that may occur due to the specific expedition tracks. Numerically, we calculate $\mathbf{R}_{SS}$ in two steps. We form a new $\mathbf{R}_{\eta\eta}$ correlation matrix that takes into account the water-mass lengthscales. Then we adjust the variance according to S_{ratio} via the equation, $\mathbf{R}_{SS} = S_{ratio}(T_{ratio} + 1)\mathbf{R}_{\eta\eta}$.

Finally, we assume that the measurement covariance, R_{MM}, is a matrix with the diagonal equal to the observational uncertainty, $\sigma_{obs} = 0.14$°C, squared (Roemmich et al., 2012).

We solve for the basinwide-average temperature profiles using a weighted and tapered least-squares formulation that minimizes,

$$J = \mathbf{q}^T\mathbf{R}_{qq}^{-1}\mathbf{q} + \mathbf{m}^T\mathbf{S}^{-1}\mathbf{m}, \tag{7}$$

where $\mathbf{R}_{qq}$ reflects the combined effect of the three types of errors (i.e., $\mathbf{R}_{qq} = \mathbf{R}_{TT} + \mathbf{R}_{SS} + \mathbf{R}_{MM}$). This least-squares weighting is chosen such that the solution coincides with the maximum likelihood estimate (assuming that the prior statistics are normally distributed and appropriately defined). Only a weak prior assumption, reflected in the weighting matrix, $\mathbf{S}$, is placed on the solution, namely that the correlation lengthscale is $L_z^{AVG} = 500$ m in the vertical, the variance is on the order of $(\sigma_S = 1°\mathrm{C})^2$, and the expected value is $< \overline{\mathbf{\Delta T}} >= 0$. The least-squares estimate is then,

$$\tilde{\overline{\mathbf{\Delta T}}} = (\mathbf{H}^T \mathbf{R}_{qq}^{-1} \mathbf{H} + \mathbf{S}^{-1})^{-1} \mathbf{H}^T \mathbf{R}_{qq}^{-1} \mathbf{\Delta T}. \tag{8}$$

The error covariance of the estimate is,

$$\mathbf{C}_{\tilde{\Delta T}} = (\mathbf{H}^T \mathbf{R}_{qq}^{-1} \mathbf{H} + \mathbf{S}^{-1})^{-1}, \tag{9}$$

where the standard error is $\boldsymbol{\sigma}_{\tilde{\Delta T}} = \sqrt{\mathrm{diag}(\mathbf{C}_{\tilde{\Delta T}})}$. This method also recovers the off-diagonal terms that correspond to the correlated errors among different parts of the basinwide-average.

Ocean heat content change

Ocean heat content change, $\Delta\mathcal{H}$, is a linear function of the temperature change and can be written as an inner vector product:

$$\Delta\mathcal{H} = \mathbf{h}^T \tilde{\overline{\mathbf{\Delta T}}}, \tag{10}$$

where $\mathbf{h}$ is a vector containing coefficients related to ocean heat capacity, seawater density, the representative area of the Indian Ocean, and the integration of temperature change over the vertical dimension. Here we integrate to a depth of $z\star = 700$ m so that we obtain heat content change from the sea surface to this depth. The Indian Ocean area is assumed to be equal to 15% of the global ocean area at all depths (ignoring the hypsometric effect).

The error covariance of $\Delta\mathcal{H}$ is an outer product,

$$\mathbf{C}_H =< (\mathbf{h}^T \tilde{\overline{\mathbf{\Delta T}}})(\mathbf{h}^T \tilde{\overline{\mathbf{\Delta T}}})^T >, \tag{11}$$

where $<>$ refers to the expected value. $\mathbf{C}_H$ is a scalar like $\Delta\mathcal{H}$. Rearranging this equation, we obtain,

$$\mathbf{C}_H = \mathbf{h}^T \mathbf{C}_{\tilde{\Delta T}} \mathbf{h}, \tag{12}$$

where $\mathbf{C}_{\tilde{\Delta T}}$ is known from the calculation of the previous section. The standard error of the heat content change is the square root of $\mathbf{C}_H$. Trends are estimated from $\Delta\mathcal{H}$ assuming the historical and WOA observations are representative of their mean observation year of 1887 and 2011, respectively.

Text S2: Errors due to line-stretch

The *Gazelle* used hemp line for profiling, which can stretch under the weight of the instruments and bottom-weight. This would tend to bias the reported *Gazelle* depths shallow, introducing a *warming* bias in the modern minus historical data. The *Valdivia* and *Planet* both used wire for profiling, which is less subject to stretch.

To assess the magnitude of this error we define two temperatures using WOA data. The first, T_{rep}, is found by interpolating the WOA data to the position and reported depth of the historical observations. The second, T_{adj}, is found by interpolating the WOA data to a stretch-corrected depth. Gebbie and Huybers (2019) compared bottom depths reported by the *Challenger* with modern bottom depths, and inferred a 4% shallow-bias in the reported depths, consistent with hemp line loaded to 25% breaking strength. We use this estimate here to correct the *Gazelle* depths. From this we can define a temperature error as $T_{err} = T_{adj} - T_{rep}$ such that positive values indicate warm biases in the modern minus historical estimates.

Profiles of T_{err} are shown in figure S3. Errors are identically zero at the surface, and increase approximately linearly down to 750 m. Below this depth the errors decrease due to the weak interior temperature gradients. The maximum error in the *Gazelle* data is estimated to be 0.31 °C at 750 m depth, however this error decreases to 0.17 °C in the basin-wide mean across all cruises (where we have assumed the wire used on the *Valdivia* and *Planet* introduces no errors in reported depth).

Text S3: Aliasing of temporal variability in the historical measurements

While the focus of this work is on multidecadal temperature variability, other timescales may be aliased into the historical observations, which could affect our estimates of 20th century temperature change. The use of data from 3 separate cruises spread over the period 1874–1907 may help alleviate this—and temporal aliasing is accounted for in the estimates of the basinwide means (section S1)—however the observations from each cruise are also not distributed uniformly through the basin (figure S1) suggesting temporal variability could alias into the observed spatial structure of the temperature change.

A prominent pattern of temperature variability here is the Indian Ocean Dipole (IOD) (N. H. Saji et al., 1999). Positive IOD events are associated with anomalously cold SST in the eastern Indian Ocean, and anomalously warm SST in the west. The pattern is reversed for negative events. Figure S4 shows the SST from ERSST reanalysis averaged over the western and eastern tropical Indian Ocean, and a Dipole Mode Index constructed from the HadSST reanalysis (N. Saji & Yamagata, 2003). The *Gazelle* sampled during the transition from a negative IOD event to neutral conditions, with a weak cool anomaly in the western tropical basin. The cruise track however was largely confined to latitudes south of 30°S, where IOD temperature anomalies are smaller (N. Saji & Yamagata, 2003). The *Planet* also sampled at the onset of a more strongly negative IOD event, with observations at low latitude where temperature anomalies are strongest. However, we note that the absolute magnitude of the temperature anomalies evident in the ERSST reanalyses were not particularly large during this period, suggesting the effect of the IOD on the *Planet* observations may be more limited than implied by the gradient-based calculation of the Dipole Mode Index. The *Valdivia* cruise was during neutral IOD conditions. Finally, we note that El-Niño-Southern Oscillation (ENSO) variability also affects Indian Ocean SST, however none of the 3 cruises appear to have been during periods of strong ENSO events (Gergis & Fowler, 2009).

Finally, to test for possible aliasing of inter-cruise variability into the zonal-mean spatial pattern (eg. figure 3) we recalculate the latitude-depth section removing one cruise at a time (figures S5, S6, and S7). From this it can be seen that, notwithstanding data gaps, the basic pattern of interior temperature change is robust to the removal of individual cruise data.

Text S4: Statistical robustness of the temperature change pattern

The historical observations are sparse, and the calculated temperature differences are noisy, such that significant averaging is required for statistical inference. However, it is also apparent that there is a striking similarity between the spatial pattern of temperature changes observed in the historical data and the late 20th century changes in the modern observational record (cf. figures 3 and 4). In the main text we therefore present the latitude-depth section of the modern minus historical temperature changes (figure 3) with bin sizes chosen principally for visual clarity, despite the observations being too underpowered to provide meaningful statistics on this scale. The consistency of the pattern seen in the historical data with multiple independent lines of evidence, as discussed in the text, provides a measure of confidence in its physical interpretation.

However, we also provide here a more rigorous assessment of the broad pattern of 20th century temperature change highlighted in the text. To do this we bin average the modern minus historical temperature change in larger bins spanning 10° of latitude, and 500 m depth (figure S8). The resulting field is broadly similar—albeit greatly smoothed— to the less heavily averaged version in the main text (figure 3). To determine regions where the null hypothesis of zero mean temperature change can be rejected it is necessary to control the false discovery rate associated with multiple hypothesis testing. We use the method outlined by Wilks (2016), where local null hypotheses are rejected if their p-values (based on the standard t test) are smaller than a threshold value, p^*,

$$p^* = \max_{i=1,\ldots,N} \left[p_{(i)} : p_{(i)} \leq (i/N)\, \alpha_{FDR} \right], \tag{13}$$

where subscripts denote the indices of the bin p-values sorted in ascending order, N is the number of bins, and α_{FDR} controls the false-discovery rate (ie. the rate at which the local null hypothesis will be incorrectly rejected). The reader is referred to Wilks (2016) for further details of the method.

Regions where the null hypothesis cannot be rejected at $\alpha_{FDR} = 0.15$ are shown in figure S8 by the stippling. This value of the α_{FDR} is relatively high, but was found to give the best balance between hypothesis testing and retaining sufficient spatial resolution to capture the features of interest (we note as well that the definition of significance in (13) is more stringent than applying individual significance calculations at each bin, such that almost all regions where the null hypothesis is rejected also have $p < 0.05$). The major features of the 20th century temperature change that are discussed in the text are in regions where the null hypothesis is rejected. This includes the strong warming near the surface along the Antarctic Circumpolar Current, moderate warming extending through the subtropical gyre interior, and cooling and warming on the poleward and equatorward flank of the thermocline dome, respectively.

We also note that for this same bin-averaging and value of α_{FDR}, the global null hypothesis (that the null hypothesis is true for all bins) cannot be rejected for the temperature differences calculated between the 1955-1964 climatology and the historical observations.

References

Gebbie, G., & Huybers, P. (2010, August). Total Matrix Intercomparison: A Method for Determining the Geometry of Water-Mass Pathways. *Journal of Physical Oceanography*, *40*(8), 1710–1728. Retrieved 2022-02-02, from `http://journals.ametsoc.org/doi/10.1175/2010JPO4272.1` doi: 10.1175/2010JPO4272.1

Gebbie, G., & Huybers, P. (2019, January). The Little Ice Age and 20th-century deep Pacific cooling. *Science*, *363*(6422), 70–74. Retrieved 2021-07-12, from `https://www.sciencemag.org/lookup/doi/10.1126/science.aar8413` doi: 10.1126/science.aar8413

Gergis, J. L., & Fowler, A. M. (2009, February). A history of ENSO events since A.D. 1525: implications for future climate change. *Climatic Change*, *92*(3-4), 343–

387. Retrieved 2021-07-17, from http://link.springer.com/10.1007/s10584-008-9476-z doi: 10.1007/s10584-008-9476-z

Gouretski, V., & Koltermann, K. (2004). *WOCE Global Hydrographic Climatology* (Tech. Rep. No. 35). Berichte des Bundesamtes für Seeschifffahrt und Hydrographie.

Huang, R. X. (2015, December). Heaving modes in the world oceans. *Climate Dynamics*, *45*(11-12), 3563–3591. Retrieved 2022-01-25, from http://link.springer.com/10.1007/s00382-015-2557-6 doi: 10.1007/s00382-015-2557-6

Roemmich, D., John Gould, W., & Gilson, J. (2012, June). 135 years of global ocean warming between the Challenger expedition and the Argo Programme. *Nature Climate Change*, *2*(6), 425–428. Retrieved 2021-07-12, from http://www.nature.com/articles/nclimate1461 doi: 10.1038/nclimate1461

Saji, N., & Yamagata, T. (2003). Possible impacts of Indian Ocean Dipole mode events on global climate. *Climate Research*, *25*, 151–169. Retrieved 2021-07-16, from http://www.int-res.com/abstracts/cr/v25/n2/p151-169/ doi: 10.3354/cr025151

Saji, N. H., Goswami, B. N., Vinayachandran, P. N., & Yamagata, T. (1999, September). A dipole mode in the tropical Indian Ocean. *Nature*, *401*(6751), 360–363. Retrieved 2021-07-16, from http://www.nature.com/articles/43854 doi: 10.1038/43854

Wilks, D. S. (2016, December). "The Stippling Shows Statistically Significant Grid Points": How Research Results are Routinely Overstated and Overinterpreted, and What to Do about It. *Bulletin of the American Meteorological Society*, *97*(12), 2263–2273. Retrieved 2021-07-22, from https://journals.ametsoc.org/doi/10.1175/BAMS-D-15-00267.1 doi: 10.1175/BAMS-D-15-00267.1

Wortham, C., & Wunsch, C. (2014, March). A Multidimensional Spectral Description of Ocean Variability. *Journal of Physical Oceanography*, *44*(3), 944–966. Retrieved 2022-02-02, from http://journals.ametsoc.org/doi/10.1175/JPO-D-13-0113.1 doi: 10.1175/JPO-D-13-0113.1

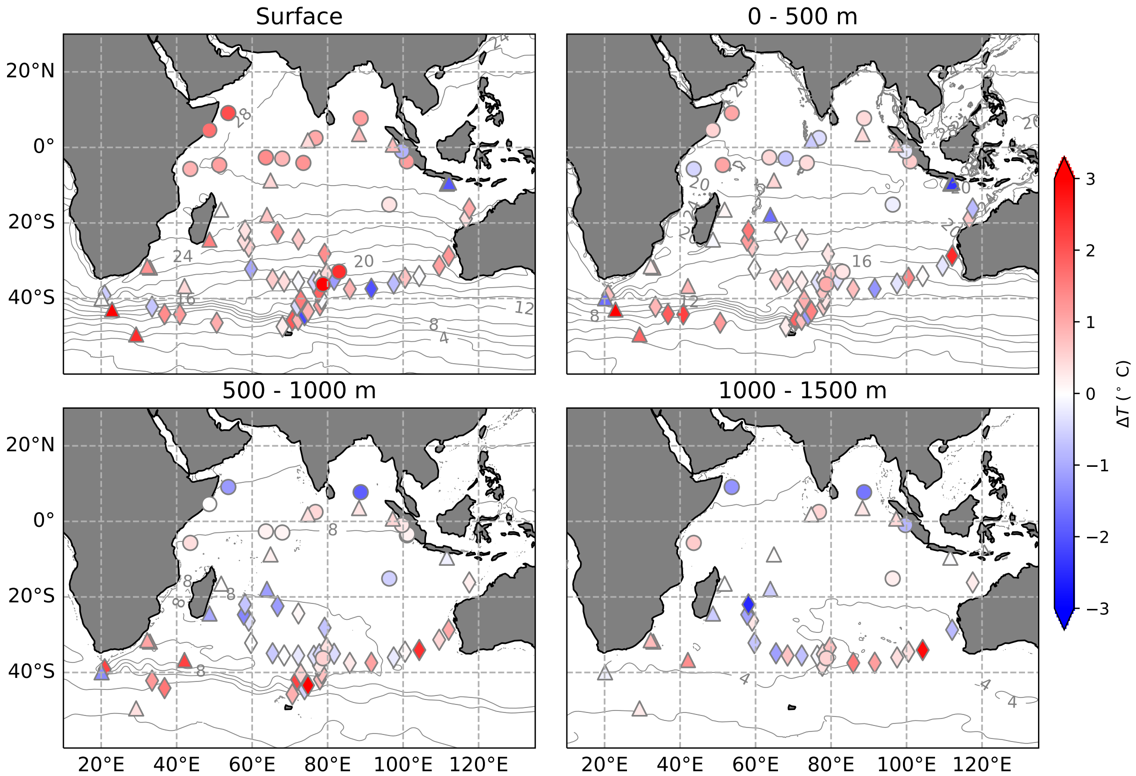

Figure S1. Depth averaged temperature change between 2005–2017 and the observations from the *Gazelle* (diamond markers), *Valdivia* (circle markers), and *Planet* (triangle markers). Depth ranges of averaging are indicated in the title of each subpanel. Modern annual average temperature values over the same depth ranges are also shown (thin contours) with a contour interval of 2°C.

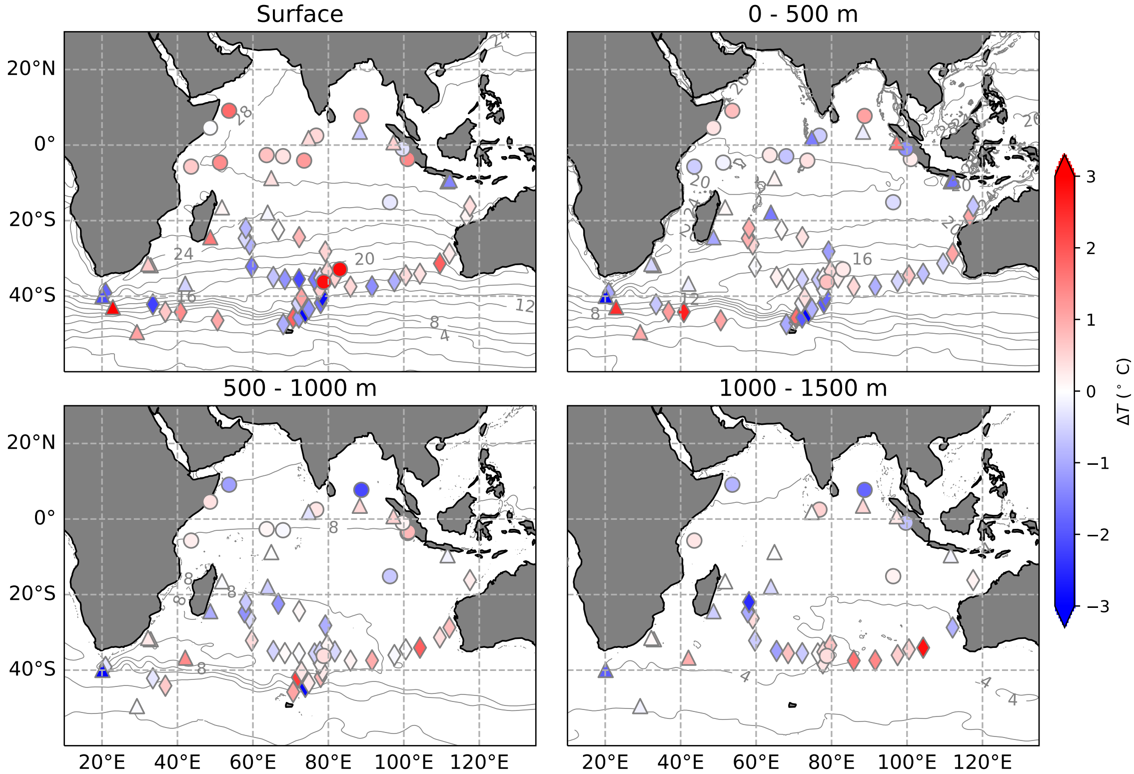

Figure S2. As in figure S1, but for the temperature differences between the 1955–1964 climatology and the historical observations.

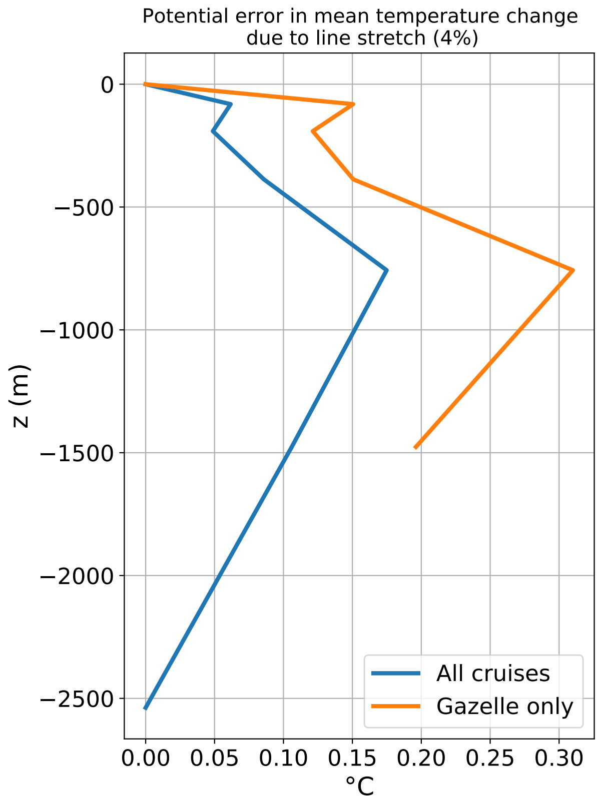

Figure S3. Depth profiles of the mean temperature bias introduced across the historical station locations by an assumed 4% shallow bias in the reported observation depths of the *Gazelle*. Positive values imply estimates of modern minus historic data are biased warm.

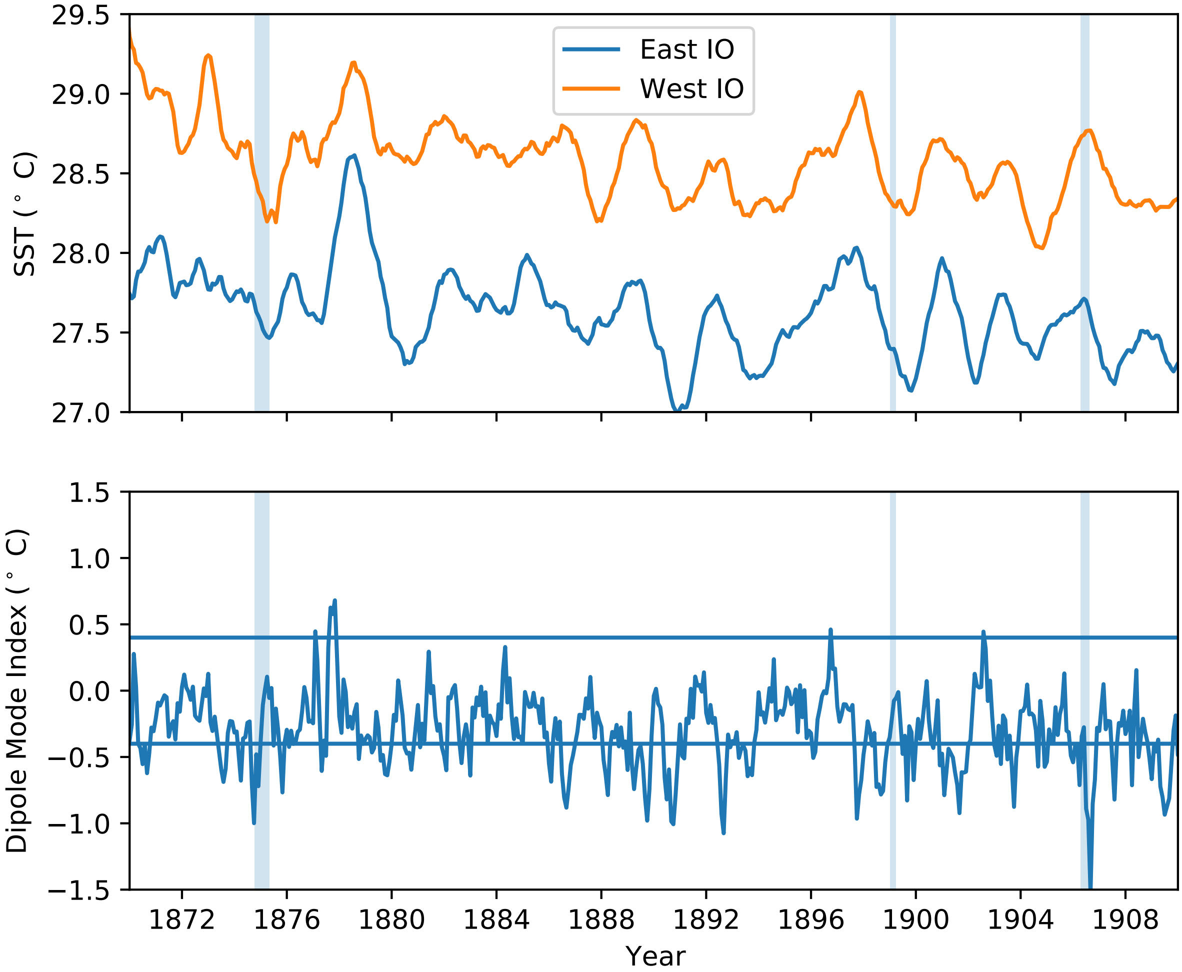

Figure S4. Top: Sea-surface temperature from ERSST averaged over the West (50°E – 70°E, 10°S – 10°N) and East (90°E – 110°E, 10°S – 0°) Indian Ocean. Bottom: The Dipole Mode Index as defined in N. Saji and Yamagata (2003, https://psl.noaa.gov/gcos_wgsp/Timeseries/DMI). In both plots the time-period of the historical cruise observations are indicated by the blue shading.

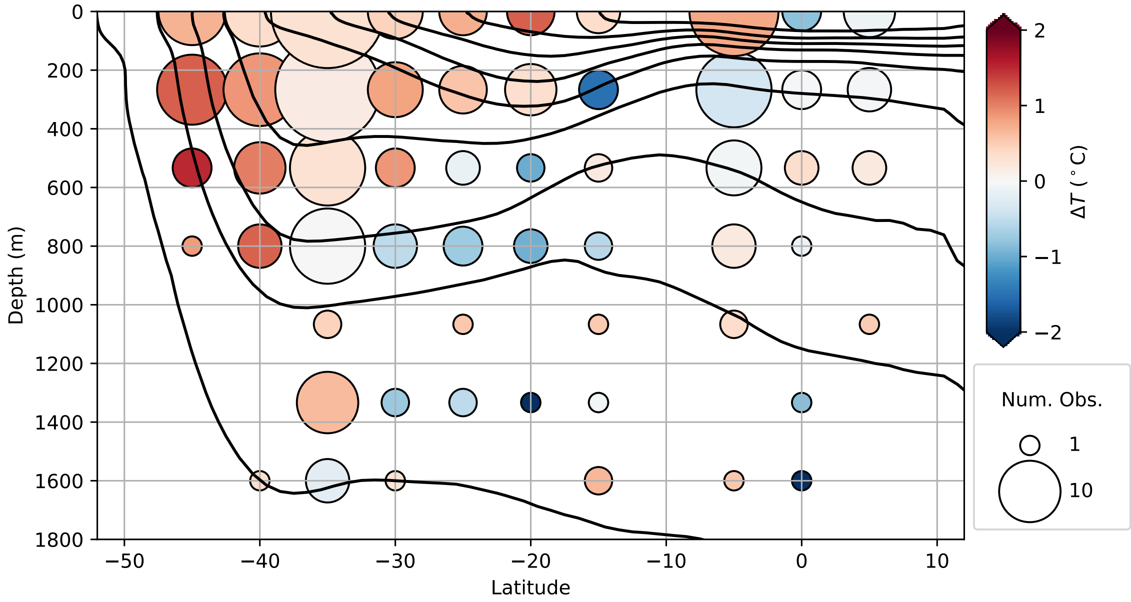

Figure S5. Latitude-depth slice of modern minus historical temperatures, as in figure 3, but without the *Planet* observations.

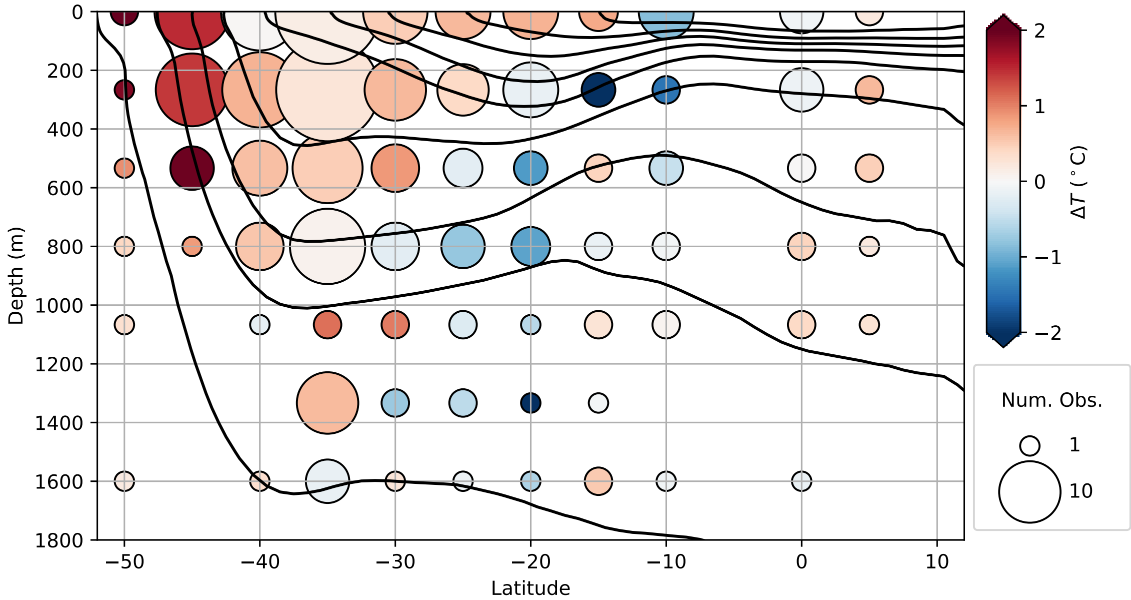

Figure S6. Latitude-depth slice of modern minus historical temperatures, as in figure 3, but without the *Valdivia* observations.

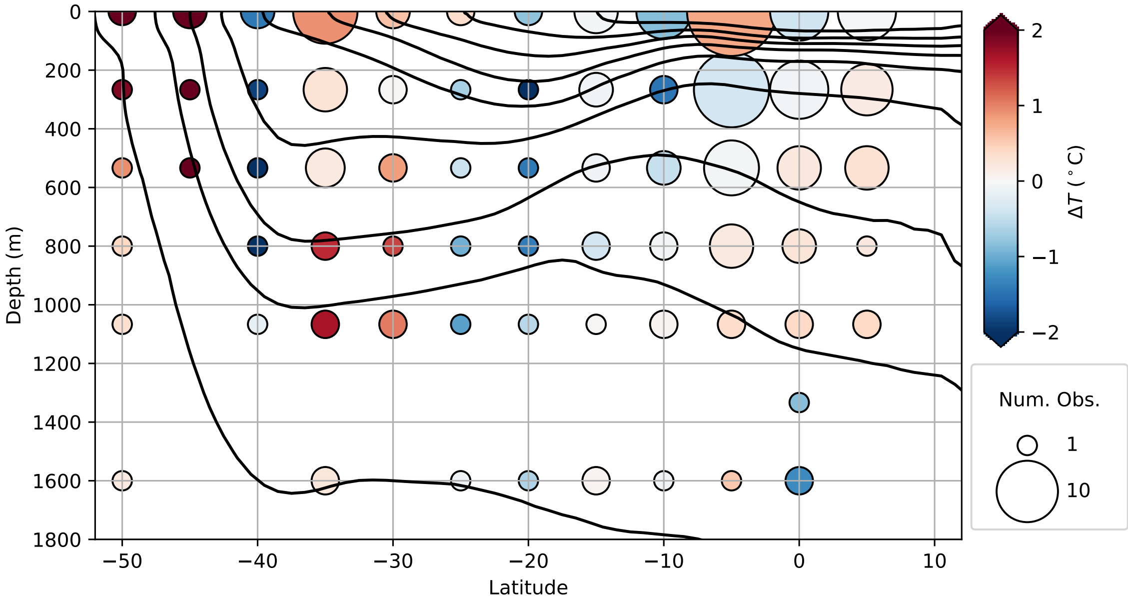

Figure S7. Latitude-depth slice of modern minus historical temperatures, as in figure 3, but without the *Gazelle* observations.

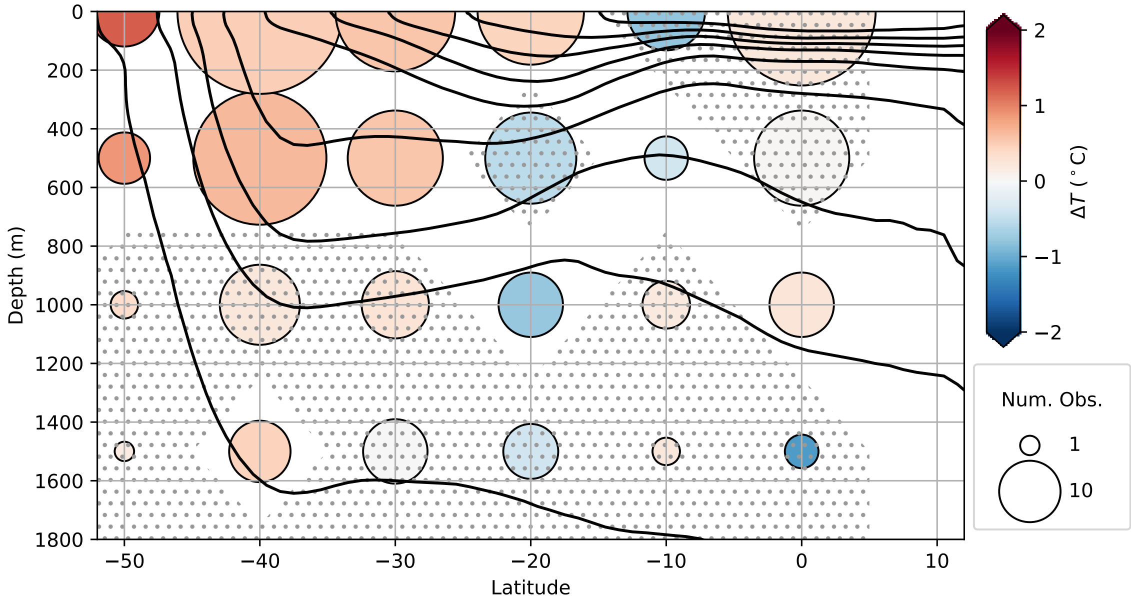

Figure S8. Latitude-depth slice of modern minus historical temperatures, as in figure 3, but averaged over larger bins. In this plot regions of stippling indicate areas where the null hypothesis of 0 mean temperature change cannot be rejected at the $\alpha_{FDR} = 0.15$ level.